Electronic Supplementary Information for:

Characterization of the [3Fe-4S]$^{0/1+}$ cluster from the D14C variant of *Pyrococcus furiosus* ferredoxin *via* combined NRVS and DFT analyses

Lars Lauterbach,*[a,b] Leland B. Gee,[a] Vladimir Pelmenschikov,*[b] Francis E. Jenney Jr,[c] Saeed Kamali,[a,d] Yoshitaka Yoda,[e] Michael W. W. Adams[f] and Stephen P. Cramer[a,g]

[a] *Department of Chemistry, University of California, Davis, CA 95616, USA*
[b] *Institut für Chemie, Technische Universität Berlin, 10623 Berlin, Germany.*
[c] *Georgia Campus, Philadelphia College of Osteopathic Medicine, Suwanee, GA 30024, USA*
[d] *Department of Mechanical, Aerospace and Biomedical Engineering, University of Tennessee Space Institute, Tullahoma, TN 37388, USA*
[e] *JASRI, SPring-8, Sayo-gun, Hyogo 679-5198, Japan*
[f] *Department of Biochemistry & Molecular Biology, Life Sciences Building, University of Georgia, Athens, GA 30602, USA*
[g] *Physical Biosciences Division, Lawrence Berkeley National Laboratory, Berkeley, CA 94720, USA*
* *Corresponding authors. E-mails: lars.lauterbach@tu-berlin.de ; pelmentschikov@tu-berlin.de*

CONTENTS

List of Figures

List of Tables

Experimental Materials and Methods

Preparation. The D14C ferredoxin from *Pyrococcus furiosus* was produced, purified, and uniformly ^{57}Fe labelled as previously described.[1] D14C (70 μM in 100 mM Tris pH 8.0) was treated and stirred aerobically with a 40 fold molar excess of $K_3[Fe(CN)_6]$ and EDTA overnight at 25°C in order to obtain the [3Fe-4S] form. The protein samples were then concentrated (Amicon Ultra-4 3 kDa MWCO, Millipore) and washed in 100 mM Tris pH 8.0 buffer. The oxidized sample was loaded into the NRVS cell directly. For reduction, the sample was treated with 100 mM Tris pH 8.0 containing 20 mM sodium dithionite in an anaerobic box by repeated washing and concentrating with Amicon Ultras. This sample was loaded into a Lucite NRVS cuvette inside the chamber and sealed with vacuum grease. All samples were immediately flash frozen in liquid nitrogen.

Mössbauer Spectroscopy. Mössbauer spectra were recorded on a SEE Co. spectrometer working in a constant acceleration mode in transmission geometry. The measurements were performed at 80 K using a Janis cryostat. A 100 mCi ^{57}Co in a Rh matrix held at room temperature (RT) was used as source. The spectra were least square fitted using Recoil software.[2] All centroid shifts, δ, are given with respect to metallic α-iron at RT. The parameters from the fittings, which are centroid shift Centroid shift (δ), quadrupole splitting (ΔE_Q, linewidth (Γ), and intensity (*I*) are summarized in Table 1.

NRVS Measurements. Nuclear resonance vibrational spectroscopy measurements were performed at SPring-8 BL09XU with a 0.8 meV energy resolution at 14.4125 keV as described previously.[3] A 4-element avalanche photo diode detector array was used to detect delayed nuclear fluorescence and K fluorescence by ^{57}Fe atoms. All measurements were performed at a 10 K reading of the cryostat sensor. The real sample temperature, as obtained from the spectral analysis, was 30–80 K. The raw data were analyzed with the PHOENIX software[4] to gain the iron partial vibrational density of states (^{57}Fe-PVDOS).

DFT Calculations

Initial coordinates for the DFT calculations were extracted from PDB 3PNI, based on the 2.8 Å resolution X-ray diffraction (XRD) analysis of the chemically oxidized *Pf* Fd D14C crystals.[5] The three Cys11/17/56 ligands to the [3Fe-4S] cluster core were modeled using $CH_3CH_2S^-$ ethylthiolates, and Cys14 of the D14C protein variant was modeled using CH_3CH_2SH ethylthiol as shown in Fig. S2. The cluster core has not been protonated, ensured by the experimental pH 8.0 conditions (protonation of the $[3Fe\text{-}4S]^0$ reduced core has been indicated for *Azotobacter vinelandii* ferredoxin I (*Av* FdI) at acidic pH < 7.0).[6] The resulting 40-atoms model complex can then be denoted as $[[Fe_3S_4](CH_3CH_2S)_3(CH_3CH_2SH)]^{3-/2-}$, respectively for the $[3Fe\text{-}4S]^{0/1+}$ cluster oxidation levels.

The broken-symmetry (BS)[7] electronic structures were constructed using an option to assign a number of unpaired α/β electrons to Fe atomic fragments, as implemented in JAGUAR 7.9.[8] These BS densities were used as starting points for geometry optimizations and analytic Hessian calculations employing harmonic approximation using GAUSSIAN 09, Revision D.01.[9] The four cysteine Cα positions, represented by methyl carbons of the $[Fe_3S_4](CH_3CH_2S)_3(CH_3CH_2SH)$ model, were fixed to their original XRD positions during geometry optimization (Fig. S2). This level of protein restraint has been found optimal in our earlier studies on the $[4Fe\text{-}4S]^{1+/2+}$ and $[4Fe\text{-}4S]^{0/1+/2+}$ cubanes from *Pf* Fd D14C and *Azotobacter vinelandii* nitrogenase Fe protein (*Av2*), respectively.[1, 10] Further protein environment of the [3Fe-4S] cluster was considered via self-consistent reaction field (SCRF) polarizable continuum model using the integral equation formalism (IEF-PCM)[11] as implemented in GAUSSIAN, with the static dielectric constant set to ε = 4.0 as often used for proteins, and the remaining IEF-PCM parameters at their default values for water. The SCRF molecular cavity was built using UFF atomic radii scaled by 1.1. Using dielectric screening with ε = 4.0 or water-like ε = 80.0 environment has been earlier shown to improve optimized structures accuracy in $[[Fe_3S_4](CH_3S)_3]^{3-}$, $[[Fe_4S_4](CH_3S)_4]^{2-}$, and $[[Fe_4S_4](CH_3CH_2S)_4]^{4-/3-/2-}$ DFT models of protein-bound clusters $[3Fe\text{-}4S]^0$, $[4Fe\text{-}4S]^{2+}$, and $[4Fe\text{-}4S]^{0/1+/2+}$, respectively;[10, 12, 13] in absence of dielectric screening (optimization in vacuum), significant negative charge of these models leads to unrealistic expansion of the Fe-S core.

In consistency with the previous study on the *Pf* Fd D14C [4Fe-4S] cluster,[1] the generalized gradient approximation (GGA) PW91[14] density functional was used for all the calculations if not otherwise mentioned. A customized B(5HF)P86[15, 16] hybrid functional based on the GGA BP86[17, 18] has been additionally used for tests on the relative energies of the BS states and electronic structures. While non-hybrid PW91 and BP86 (0% of Hartree-Fock exchange) are known to perform well on Fe-S cluster geometries and normal modes,[12, 16, 19-21] a calibrated level of 5% Hartree-Fock exchange in the customized B(5HF)P86 functional has been indicated to give optimal description of covalency in Fe-S clusters.[15, 16]

The LACV3P** basis set as implemented in JAGUAR was used for all the calculations, implying a 6-311G** triple-ζ basis set including polarization function for the 1st- and 2nd-row elements. For the Fe atom, LACV3P** uses the Los Alamos effective core potential (ECP), and the valence part is essentially of triple-ζ quality. Relevant to NRVS, the ^{57}Fe isotope mass was used for the normal mode analysis following Hessian calculations. Based on the normal mode outputs from GAUSSIAN, ^{57}Fe partial vibrational density of states (^{57}Fe-PVDOS) and kinetic energy distribution (KED) spectral profiles were generated using Q-SPECTOR, an in-house Python tool successively applied as well earlier.[1, 10, 22-25] To empirically account for the resolution of the present NRVS experiment, the simulated spectra were broadened by convolution with a FWHM = 14 cm^{-1} Lorentzian.

Mössbauer Spectroscopy Results

The [3Fe-4S] clusters show two physiological redox states. The oxidized form of the cluster $[3Fe\text{-}4S]^{1+}$ has the electronic spin of $S = 1/2$, which results from spin-frustrated coupling of three high-spin ferric ($S = 5/2$) ions. The reduced $[3Fe\text{-}4S]^{0}$ form has a $S = 2$ ground state due to antiferromagnetic coupling of the ferric ion to two mixed-valent ($Fe^{2.5+}$) ions ($S = 9/2$).[26, 27]

Mössbauer spectra were measured on oxidized and reduced samples of D14C within the same sample cuvette as for NRVS. The spectrum from the oxidized sample exhibits one doublet (see Fig. S1). Due to the asymmetry of the lines, the spectrum is fitted with two doublets with close lying hyperfine parameters. The 1st component has δ = 0.257 mm/s and ΔE_Q = 0.534 mm/s. The 2nd component has δ = 0.328 mm/s and ΔE_Q = 0.638 mm/s. The widths are 0.30 mm/s and 0.41 mm/s, respectively. These parameters are typical for high-spin Fe^{3+} with thiolate ligands in tetrahedral geometry. It is worth-mentioning that the reason for having two subspectra is due to the different environments for Fe atoms. Although the electronic structure for all atoms is the same, i.e. being in the high-spin Fe^{3+}, the slightly different ligands and/or small differences of the charge distributions at different Fe atoms give rise to different quadrupole splitting, resulting in the asymmetry in the spectrum. This shows all three irons of the [3Fe-4S] cluster have the same redox state in its oxidized state. Reduction by one electron by dithionite results in a $S = 2$ state. The Mössbauer spectrum for the reduced cluster consists of three doublets. The 1st doublet has δ = 0.307 mm/s and ΔE_Q = 0.475 mm/s, which are typical values for high-spin Fe^{3+}. The 2nd doublet has δ = 0.446 mm/s and ΔE_Q = 1.396 mm/s, representing a valence-delocalized $Fe^{2.5+}$ pair with a shared electron between two irons.[27, 28] The ratio of these components is 1:2. The 3rd doublet, X, has δ = 0.403 mm/s and ΔE_Q = 0.406 mm/s. The values are close to the values for the weighted average between Fe^{3+} and $Fe^{2.5+}$. Previous Mössbauer studies on Fe-S cluster suggest that this species represent a fully delocalized state with one electron equally spread over all three irons,[27] with a temperature-dependent contribution. The intensity of this component, 24%, is in the range of the previous study.[27] The comparison of our results with Mössbauer spectra of the [4Fe-4S] form of *Pf* Fd D14C from an earlier study[1] reveals that the oxidized and the reduced sample are in a homogenous state and the conversion of the [4Fe-4S] to [3Fe-4S] form was complete.

[3Fe-4S] Cluster: Spin Coupling

As disclosed previously,[26, 27, 29] a [2Fe↑:1Fe↓] spin-coupling pattern applies to both oxidation levels of the [3Fe-4S] cluster considered here, where '↑' and '↓' respectively denote $M_{Si} > 0$ and $M_{Si} < 0$ for the spin-projection values of the Fe*i* iron site spins S_i, i = 1,2,3. Three combinations are available for the [2Fe↑:1Fe↓] broken-symmetry (BS) pattern distribution among the three Fe ions. These BS states can be named as BS12, BS13, and BS23 after the Fe*i* numbers of the two spin-up sites ([2Fe↑]); here, the Fe*i* numbering scheme follows Figs. 1 and S2. At the $[3Fe\text{-}4S]^{0/1+}$ oxidation levels, the relative energies between the three structurally optimized BS states are respectively within 1.0/0.2 kcal/mol using PW91 and within 0.5/0.2 kcal/mol using B(5HF)P86 DFT functionals (Table S2). Because these energy differences are within the inherent accuracy limits of DFT, they cannot provide a conclusive preference to any of the three BS states. A comparison of the observed and BS-dependent calculated ^{57}Fe-PVDOS spectra in Fig. S4 does not favor particular BS state either. BS12, which has the lowest energy in most of the cases (except the PW91 calculation on $[3Fe\text{-}4S]^{1+}$), has been regarded as the representative spin configuration reported in this study; see further support for BS12 below.

A strong inhomogeneity of Fe*i* spin densities (which approximate the M_{Si} values) reported in Table S2 for the $[3Fe\text{-}4S]^{1+}$ (S = 1/2) oxidized cluster is indicative of spin-frustration (which implies S_i vector orientations different from parallel or antiparallel) between the three high-spin ferric (Fe^{3+}, d^5, S = 5/2) iron sites; for the computed $[3Fe\text{-}4S]^{1+}$ Fe1/2/3 spin densities of BS12, we note a qualitative correspondence to the A_i = 5/18/-41 MHz isotropic parts of the Fe*i* magnetic hyperfine interaction tensors observed for $[3Fe\text{-}4S]^{1+}$ from *Av* FdI.[26] In contrast, Fe*i* spin densities obtained for the $[3Fe\text{-}4S]^{0}$ (S = 2) reduced cluster are largely homogeneous in their magnitudes; accepting for moderate spin density deviations from their intrinsic values within the cluster, the BS12 solution here corresponds to a (ferromagnetic) mixed-valence pair formed by Fe1 and Fe2 ($Fe^{2.5+}$, S = 9/4), coupled antiferromagnetically to ferric Fe3.[27] Provided the Fe sites permutation, solutions received for BS13 and BS23 bear their qualities similar to BS12 at both $[3Fe\text{-}4S]^{0/1+}$ oxidation levels (Table S2). Finally, PW91 and B(5HF)P86 provide qualitatively similar electronic structures, with magnitudes of Fe*i* spin densities somewhat higher from the hybrid B(5HF)P86 functional.

Via combination of EPR, variable-temperature magnetic circular dichroism (VTMCD), and sequence specific ^{1}H NMR spectroscopies, the identity of the noncoordinating residue equivalent to position 14 in *Pf* Fd has been indicated as a determinant in the location of the reducible pair of irons in [3Fe-4S] clusters of wild-type and mutant ferredoxins.[30, 31] This residue is at position X(II) of the conserved C(I)-X-X-X(II)-X-X-C(III) polypeptide cluster binding motif; for *Pf* Fd D14C, C(I) = Cys11, X(II) = Cys14, and C(III) = Cys17. For the X(II) = C(II) = Cys case, it has been concluded that the two Fe coordinated by C(I) and C(III) cysteines form the reducible pair, and the remaining Fe coordinated by cysteine outside the conserved motif (here, Cys56) is a 'unique' site.[30, 31] Our selection of BS12 to underlie the representative DFT results (see above) is then consistent with the outlined spectroscopic indication: Fe1 and Fe2 form the reducible pair, and Fe3 remains 'unique' high-spin ferric in $[3Fe\text{-}4S]^{0/1+}$ of *Pf* Fd D14C.

[3Fe-4S] Cluster: Structural Aspects

Trends in redox-dependent structural shifts in the *Pf* Fd D14C [3Fe-4S]/[4Fe-4S] clusters, well mapped by observed and DFT-simulated NRVS (^{57}Fe-PVDOS) vibrational properties, are discussed in the main text employing averaged Fe–Fe/S_t/S_b internuclear distances from DFT optimization. This section extends to a comparison of the optimized *Pf* Fd D14C $[3Fe\text{-}4S]^{0/1+}$ structures to relevant experimental data collected in Table S3; for the [4Fe-4S] cluster from the very same protein, this type of comparison has been carried out earlier.[1]

The only available X-ray diffraction (XRD) structure PDB 3PNI[5] of specifically *Pf* Fd D14C variant is for the oxidized protein and has been presently used as a starting point for the corresponding $[3Fe\text{-}4S]^{1+}$ DFT modeling. A critical assessment of the DFT structure quality is however problematic here due to a relatively low 2.8 Å resolution of its experimental source, PDB 3PNI. We note that the DFT optimization leads to a consistent mean Fe–Fe/S_t/S_b distances expansion by respectively 0.05/0.05/0.04 Å (Table S3). Interestingly, higher 1.5 Å resolution data on the oxidized wild-type (WT) *Pf* Fd variant from PDB 1SJ1[32] shows notable expansion of the cluster, as compared to PDB 3PNI. A critical assessment is impeded here as well due to residual electron density in PDB 1SJ1, observed at location of the missing 4th Fe site; notably, the averaged Fe–Fe/S_t/S_b distances from PDB 1SJ1 better match those from our DFT modeling on *Pf* Fd D14C $[4Fe\text{-}4S]^{2+/1+}$.

As already discussed in the main text, high 1.4 Å resolution determinations PDB 6FD1/6FDR of respectively $[3Fe\text{-}4S]^{0/1+}$ forms of *Azotobacter vinelandii* ferredoxin (*Av* FdI) displayed structural deviations within experimental error only.[33, 34] Collectively, these two *Av* FdI structures are in better agreement with our DFT modeling of the reduced *Pf* Fd D14C $[3Fe\text{-}4S]^0$ cluster. For the $[3Fe\text{-}4S]^0$ case, the averaged Fe–Fe/S_t/S_b distances are different by respectively 0.0/0.06/0.04 Å when comparing the *Av* FdI PDB 6FD1 to our DFT modeling (Table S3).

High-resolution XRD data on a synthetic compound hosting the reduced $[Fe_3S_4]^0$ cluster[35] provides the most consistent match to our $[3Fe\text{-}4S]^0$ DFT structure: here, experiment-to-DFT shift in averaged Fe–Fe/S_t/S_b distances is respectively -0.02/0.02/0.02 Å only (Table S3). A comparable level of structural quality has been achieved in an earlier DFT study on the $[3Fe\text{-}4S]^0$ cluster,[12] where the best computational protocol delivered mean absolute error of 0.016 Å in Fe–S bonding distances, as compared to the synthetic $[Fe_3S_4]^0$ species.

A separate comment goes to the Fe–Fe distances distribution, well recognized to be dependent on spin configuration (among other factors, such as protein environment) in Fe-S clusters. While in the all-ferric $[3Fe\text{-}4S]^{1+}$ cluster the optimized Fe–Fe distances are essentially homogeneous and distribute within 0.03 Å only, for the reduced $[3Fe\text{-}4S]^0$ cluster spin-dependent delocalization in the mixed-valence [$Fe^{2.5+}\uparrow$-$Fe^{2.5+}\uparrow$] pair leads to the corresponding short Fe1–Fe2 distance, as compared to 0.07-0.08 Å longer Fe1/2–Fe3 distances in the two [$Fe^{2.5+}\uparrow$-$Fe^{3+}\downarrow$] pairs (Table S3). This is consistent with the BS12 spin configuration clarified in the previous section. The outlined 'one short / two long' Fe–Fe distances pattern for $[3Fe\text{-}4S]^0$ has been resolved in the synthetic $[Fe_3S_4]^0$ species XRD structure as well.[35]

[3Fe-4S] Cluster: Reorganization Energies

The present analysis focuses on λ_i self-exchange inner-sphere contribution to the reorganization energy λ of the *Pf* Fd D14C $[3Fe\text{-}4S]^{0/1+}$ cluster. Here, the inner-sphere implies the cluster inorganic core and its first coordination sphere, represented by the DFT model. Calculation of λ_i was done in a manner following Ryde et al[36, 37] and others[1, 12, 19, 21]:

$$\lambda_i = \lambda_{ox} + \lambda_{red}$$

$$\lambda_{ox} = E(Ox^{Ox}) - E(Red^{Ox})$$

$$\lambda_{red} = E(Red^{Red}) - E(Ox^{Red})$$

where λ_{ox}, the reorganization energy during oxidation, is the difference between the energies of the oxidized complex in its equilibrium geometry (Ox^{Ox}) and oxidized complex at the equilibrium structure of the reduced complex (Red^{Ox}). Similarly, the λ_{red} reorganization energy during reduction is the difference between the energies of the reduced complex in its equilibrium geometry (Red^{Red}) and reduced complex at the equilibrium structure of the oxidized complex (Ox^{Red}).

The representative spin configuration BS12 (as detailed above) has been selected for the *Pf* Fd D14C $[3Fe\text{-}4S]^{0/1+}$ cluster reorganization energy assessment, and the values computed are collected as $BS12_\lambda$ (kcal/mol) in Table S2. These values translate to λ_{ox} = 52.7, λ_{red} = 58.6, and λ_i = 111.3 kJ/mol using the PW91 functional; alternative application of the B(5HF)P86 functional leads to a very similar result of λ_{ox} = 51.9, λ_{red} = 60.7, and λ_i = 112.5 kJ/mol. A previous study on the *Pf* Fd D14C $[4Fe\text{-}4S]^{1+/2+}$ cluster employing the equivalent DFT protocol provided λ_i = 18.8 kJ/mol.[1] Within the very same *Pf* Fd D14C protein framework, our results therefore indicate 113.3/18.8 ≈ 6 higher reorganization energy of the $[3Fe\text{-}4S]^{0/1+}$ cluster as compared to the $[4Fe\text{-}4S]^{1+/2+}$ variant.

We note that reorganization energies calculated for Fe–S clusters vary significantly depending on the computational protocol and environment treatment, as discussed earlier.[1, 12, 21] λ_i = 67 kJ/mol has been reported for a generic $[3Fe\text{-}4S]^{0/1+}$ cluster,[12] and broad range of λ_i ≈ 18 to 50 kJ/mol is available from the literature on $[4Fe\text{-}4S]^{1+/2+}$.[21, 37, 38] Notably, our modeling of *both* [3Fe-4S] and [4Fe-4S] clusters from *Pf* Fd D14C included (*i*) all four Cys ligands (as shown in Fig. S2) coordinating the [4Fe-4S] variant prior to its oxidative damage, (*ii*) Cα carbon fixations to their original XRD positions, and (*iii*) implicit protein environment; the outer-sphere λ_o contribution to the reorganization energy is then partially accounted as well. This adds extra confidence in relative assessment of the *Pf* Fd D14C $[3Fe\text{-}4S]^{0/1+}$ and $[4Fe\text{-}4S]^{1+/2+}$ clusters reorganization energies as given above.

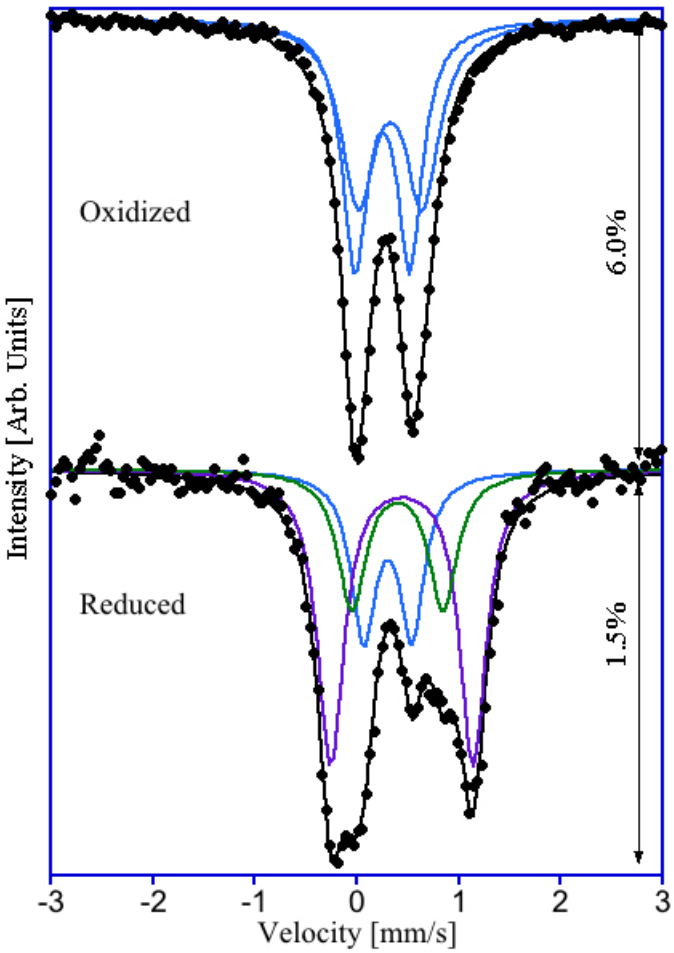

Fig. S1 Mössbauer spectra of [3Fe-4S]-containing *Pf* Fd D14C recorded at 80 K. Black circles represent oxidized and reduced D14C experimental Mössbauer data. The subspectra are Lorentzian doublets of Fe^{3+} (blue), $Fe^{2.5+}$ (violet) and species X (green, see text and Table S1 for details). The sum of subspectra is shown in black lines.

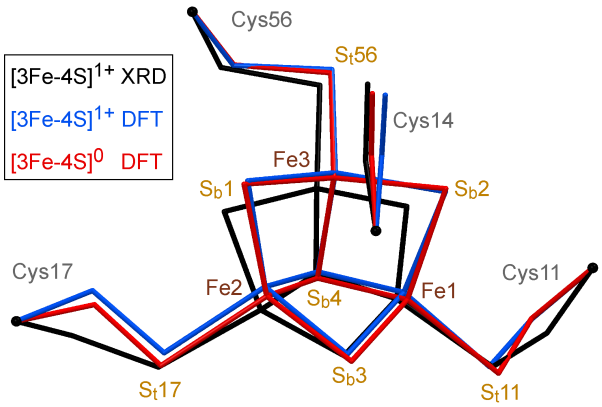

Fig. S2 Overlay of the *Pf* Fd D14C $[3Fe\text{-}4S]^{1+}$ cluster reference PDB 3PNI[5] XRD structure (black) with the DFT model optimized at the $[3Fe\text{-}4S]^{1+}$ oxidized (blue) and $[3Fe\text{-}4S]^{0}$ reduced (red) levels. The Fe/S atom labels are given in brown/yellow, respectively. Hydrogen atoms are omitted for clarity, and Cys14 sulfur is protonated. The four cysteine alpha-carbons fixed to their original crystallographic positions during the optimization are marked with black spheres. All models are shown in 0.05 Å radius tubes.

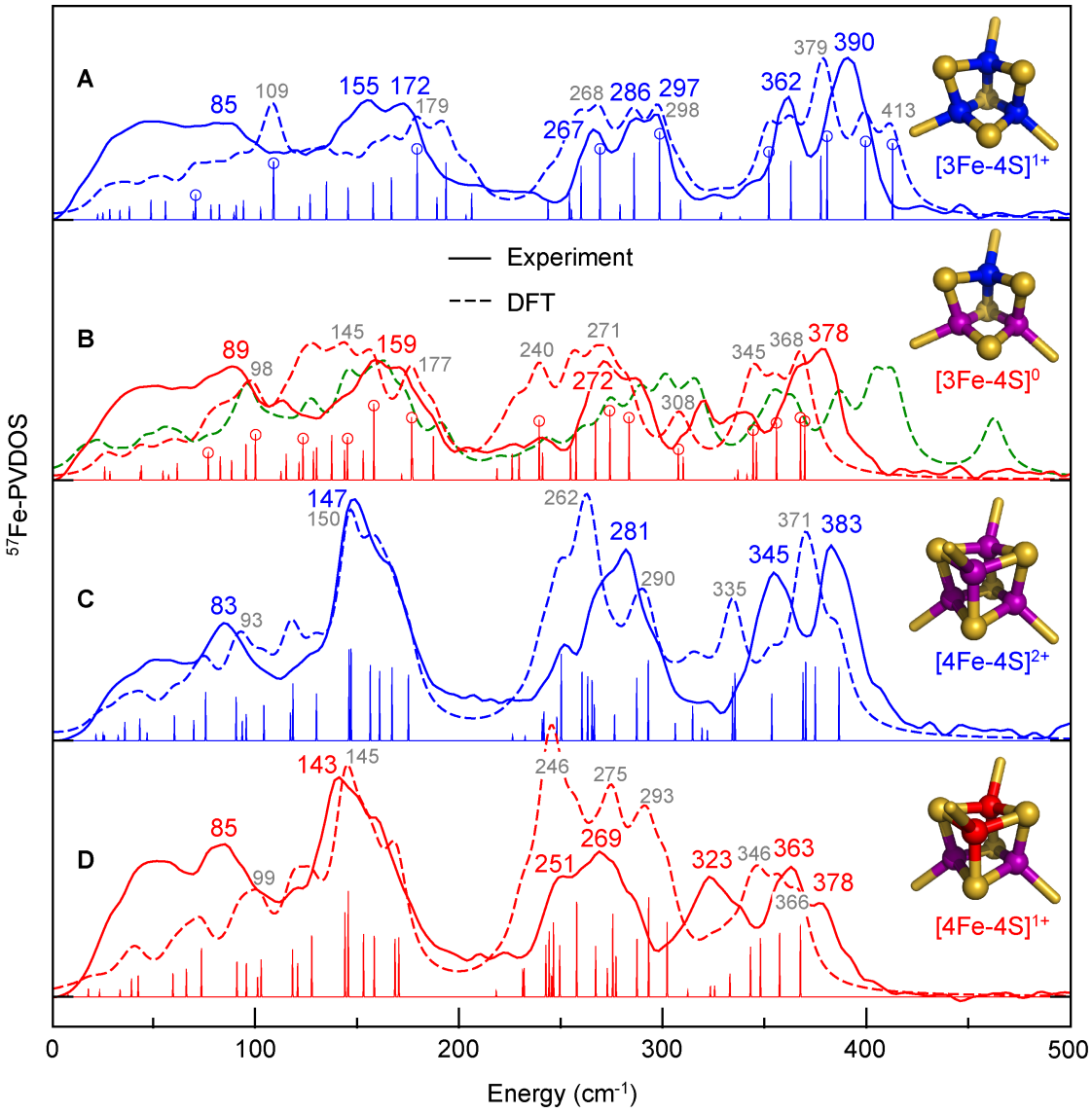

Fig. S3 Overlay of the observed NRVS (solid line) and representative DFT-calculated (broken line) ^{57}Fe-PVDOS spectra for the ^{57}Fe-enriched [3Fe-4S] and [4Fe-4S] variants of *Pf* Fd D14C at the reduced and oxidized levels. The non-broadened intensities (and normal mode positions) from DFT are given in stick-style. On right, electronic structures of the Fe-S clusters are schematically shown, where $Fe^{3+/2.5+/2+}$ are in blue/purple/red, respectively, and sulfide ligands are in yellow. *Top to bottom*: $[3Fe\text{-}4S]^{1+}$ (A); $[3Fe\text{-}4S]^{0}$ (B); $[4Fe\text{-}4S]^{2+}$ (C); $[4Fe\text{-}4S]^{1+}$ (D). For the selected $[3Fe\text{-}4S]^{0/1+}$ normal modes labeled with circles (A,B), animated GIF files are available as separate part of ESI†. In (B), the green line corresponds to the reduced $[3Fe\text{-}4S]^{0}$ state DFT modeling using the equilibrium structure of the oxidized $[3Fe\text{-}4S]^{1+}$ state. The data on the [4Fe-4S] variant have been in part published previously.[1]

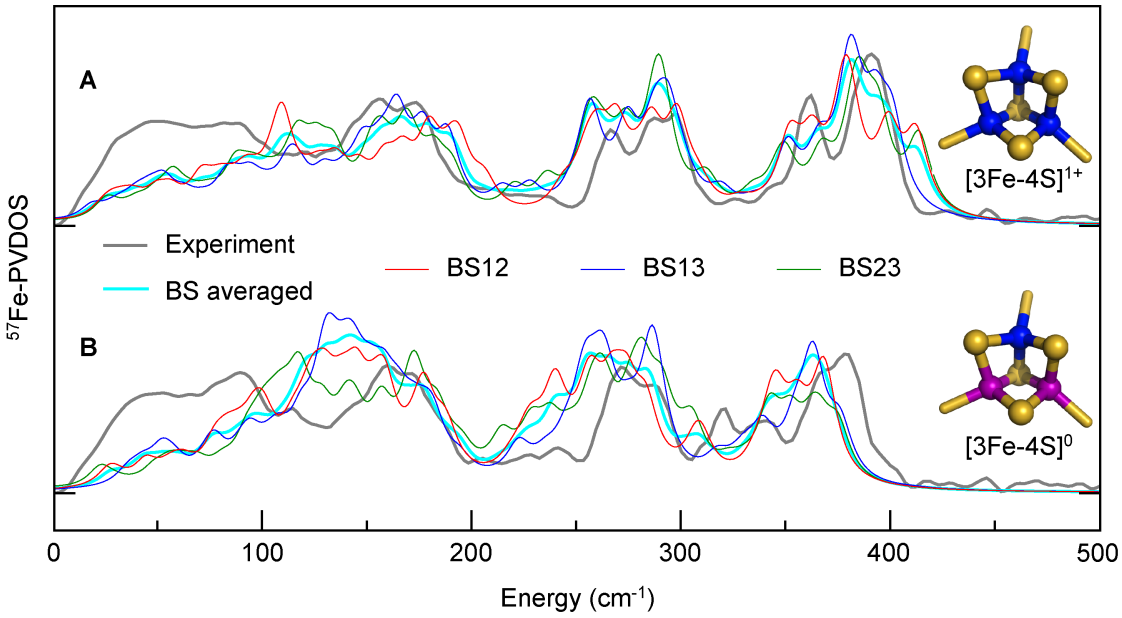

Fig. S4 Overlay of the observed NRVS and broken-symmetry (BS) state variants of the DFT-calculated ^{57}Fe-PVDOS spectra for the ^{57}Fe-enriched [3Fe-4S] *Pf* Fd D14C at the oxidized $[3Fe\text{-}4S]^{1+}$ (A) and reduced $[3Fe\text{-}4S]^{0}$ (B) levels. The experimental line is in grey, BS12 in red, BS13 in blue, BS23 in green, and arithmetic mean from the three BS states spectra is in cyan. BS12 is the representative DFT solution used to report [3Fe-4S] *Pf* Fd D14C spectra elsewhere in this study (Figs. 2 and S3). On right, electronic structures of the [3Fe-4S] cluster are schematically shown, where $Fe^{3+/2.5+/2+}$ are in blue/purple/red, respectively, and sulfide ligands are in yellow.

Table S1 Mössbauer parameters for the iron sites of the oxidized and reduced [3Fe-4S] cluster. Centroid shift (δ), quadrupole splitting (ΔE_Q), Lorentzian linewidth (Γ) and intensities (I) are shown.

	Type and S_{tot}	δ (mm/s)	ΔE_Q (mm/s)	Γ_1 (mm/s)	I (%)
ox. D14C	$[3Fe\text{-}4S]^{1+}$				
Fe^{3+}	$S = 1/2$	0.257	0.534	0.30	50
Fe^{3+}		0.328	0.638	0.41	50
red. D14C	$[3Fe\text{-}4S]^{0}$				
Fe^{3+}	$S = 2$	0.307	0.475	0.29	26
$Fe^{2.5+}$		0.446	1.396	0.32	49
species X		0.403	0.896	0.33	25

Table S2 Relative energies in three broken-symmetry (BS) states and Mulliken spin populations for the three iron sites of the *Pf* Fd D14C $[3Fe\text{-}4S]^{0/1+}$ cluster from DFT calculations using PW91 (top) and B(5HF)P86 (bottom) functionals.[a]

	Relative Energy (kcal/mol) and Spin Population (*e*)							
	$[3Fe\text{-}4S]^{1+}$				$[3Fe\text{-}4S]^{0}$			
	BS12	**$BS12_\lambda$**[d]	**BS13**	**BS23**	**BS12**	**$BS12_\lambda$**[d]	**BS13**	**BS23**
				PW91				
Energy[b]	0.0	*+12.6*	+0.7	+1.0	0.0	*+14.0*	-0.1	-0.2
Fe1[c]	1.50	*1.37*	2.55	-3.02	3.34	*3.06*	3.31	-3.28
Fe2[c]	2.49	*2.98*	-3.13	1.20	3.35	*3.15*	-3.30	3.32
Fe3[c]	-3.13	*-3.23*	1.44	2.83	-3.31	*-3.16*	3.35	3.34
				B(5HF)P86				
Energy[b]	0.0	*+12.4*	+0.5	0.0	0.0	*+14.5*	+0.1	+0.2
Fe1[c]	1.80	*1.89*	2.87	-3.25	3.43	*3.25*	3.41	-3.42
Fe2[c]	2.68	*3.01*	-3.33	1.33	3.44	*3.22*	-3.44	3.42
Fe3[c]	-3.34	*-3.42*	1.52	3.05	-3.44	*-3.34*	3.44	3.43

[a] The DFT results from PW91 are representative and implied elsewhere, if not otherwise mentioned.

[b] Energies (kcal/mol) are relatively to BS12 at both oxidation levels.

[c] Fe sites labeling for Mulliken spin populations (*e*) corresponds to Figs. 1 and S2.

[d] $BS12_\lambda$ correspond to states Ox^{Red}/Red^{Ox} of the $[3Fe\text{-}4S]^{0/1+}$ cluster used for the $\lambda_{red/ox}$ reorganization energies calculation, respectively, as explained in the text.

Table S3 Fe–Fe and bonding Fe–S internuclear distances (Å) in selected ferredoxin [3Fe-4S] and [4Fe-4S] clusters and $[Fe_3S_4(LS_3)]^{3-}$ model compound from X-ray diffraction (XRD) data analysis and DFT geometry optimization.[a]

	Internuclear Distance (Å)					
	XRD[b]	XRD[c]	XRD[d]	XRD[e]	DFT[f]	DFT[g]
	$[Fe_3S_4(LS_3)]^{3-}$	*Av* FdI	*Pf* Fd WT	*Pf* Fd D14C	*Pf* Fd D14C	*Pf* Fd D14C
	$[Fe_3S_4]^0$	$[3Fe\text{-}4S]^{1+/0}$	$[3Fe\text{-}4S]^{1+}$	$[3Fe\text{-}4S]^{1+}$	$[3Fe\text{-}4S]^{1+/0}$	$[4Fe\text{-}4S]^{2+/1+}$
			Fe – Fe			
Fe1 – Fe2	2.67	2.64 / 2.65	2.65	2.53	2.61 / 2.63	
Fe1 – Fe3	2.73	2.73 / 2.73	2.71	2.56	2.60 / 2.70	
Fe2 – Fe3	2.71	2.67 / 2.65	2.75	2.54	2.61 / 2.71	
Fe – Fe	2.70	2.68 / 2.68	2.70	2.54	2.61 / 2.68	2.68 / 2.70
			Fe – S_t (terminal cysteinates)			
Fe1 – S_t11	2.33	2.31 / 2.30	2.28	2.18	2.21 / 2.35	
Fe2 – S_t17	2.32	2.32 / 2.28	2.32	2.18	2.24 / 2.35	
Fe3 – S_t56	2.31	2.29 / 2.26	2.23	2.21	2.27 / 2.32	
Fe – S_t	2.32	2.31 / 2.28	2.28	2.19	2.24 / 2.34	2.27 / 2.32
			Fe – S_b (bridging inorganic)			
Fe1						
– S_b2	2.25	2.29 / 2.21	2.32	2.24	2.17 / 2.27	
– S_b3	2.28	2.28 / 2.32	2.17	2.18	2.15 / 2.32	
– S_b4	2.33	2.32 / 2.32	2.33	2.10	2.23 / 2.38	
Fe1 – S_b	2.29	2.30 / 2.28	2.27	2.17	2.18 / 2.32	
Fe2						
– S_b1	2.25	2.21 / 2.20	2.26	2.23	2.21 / 2.26	
– S_b3	2.27	2.28 / 2.29	2.25	2.21	2.20 / 2.33	
– S_b4	2.31	2.33 / 2.33	2.31	2.10	2.27 / 2.37	
Fe2 – S_b	2.28	2.27 / 2.27	2.27	2.18	2.23 / 2.32	
Fe3						
– S_b1	2.24	2.21 / 2.23	2.24	2.21	2.23 / 2.26	
– S_b2	2.27	2.23 / 2.24	2.34	2.19	2.24 / 2.25	
– S_b4	2.27	2.27 / 2.23	2.38	2.13	2.32 / 2.31	
Fe3 – S_b	2.26	2.24 / 2.23	2.32	2.18	2.26 / 2.27	
Fe – (μ_2)S_b1/2/3	2.26	2.25 / 2.25	2.26	2.21	2.20 / 2.28	
Fe – (μ_3)S_b4	2.31	2.31 / 2.29	2.34	2.11	2.27 / 2.35	
Fe – S_b	2.28	2.27 / 2.26	2.29	2.18	2.22 / 2.30	2.27 / 2.28
			Fe – $S_{t/b}$			
Fe – $S_{t/b}$	2.29	2.28 / 2.27	2.29	2.18	2.23 / 2.31	2.27 / 2.29

[a] Atom labeling corresponds to Figs. 1 and S2. The arithmetic mean distances are shadowed with grey fields.
[b] High-resolution data on $[Fe_3S_4(LS_3)]^{3-}$ synthetic compound.[35] The atom labeling correspondence (present to ref.[35]) is Fe1/2/3 to Fe(3/1/2); S_b1/2/3/4 to S(3/4/2/1); S_t11/17/56 to S(31/11/21).
[c] 1.4 Å resolution data on Azotobacter vinelandii ferredoxin from PDB 6FD1/6FDR.[33, 34] The atom labeling correspondence (present to ref.[33]) is Fe1/2/3 to Fe2/3/1; S_b1/2/3/4 to S2/3/1/4; S_t11/17/56 to Sγ16/49/8.
[d] 1.5 Å resolution data on wild-type *Pf* Fd variant from PDB 1SJ1.[32]
[e] 2.8 Å resolution data on D14C *Pf* Fd mutant from PDB 3PNI.[5]
[f] This work. Representative BS12 structures are reported.
[g] Selected mean distances from earlier *Pf* Fd D14C [4Fe-4S] DFT modeling.[1]

Table S4 Cartesian coordinates (Å) and total absolute energies (Hartree) of the *representative* DFT-optimized models using PW91 functional and BS12 broken-symmetry state.

Oxidized *Pf* Fd D14C [3Fe-4S]$^{1+}$ model $[[Fe_3S_4](CH_3CH_2S)_3(CH_3CH_2SH)]^{2-}$	**Reduced *Pf* Fd D14C [3Fe-4S]^{0} model** $[[Fe_3S_4](CH_3CH_2S)_3(CH_3CH_2SH)]^{3-}$
40 Absolute Energy: -3874.161016 Fe 4.459172 9.256593 17.254875 Fe 3.989838 11.643482 16.317570 Fe 5.215857 11.345545 18.603257 S 2.734810 9.849057 16.108846 S 4.259182 9.484077 19.403911 S 6.030154 10.662907 16.536625 S 3.655326 12.897832 18.105363 C 6.183984 6.164044 18.836942 C 6.348704 6.692845 17.414778 S 4.750331 7.165568 16.595934 H 5.729712 6.934743 19.476113 H 6.999492 7.578032 17.401466 H 6.806609 5.931721 16.763523 H 5.536318 5.275530 18.856726 H 7.161729 5.889487 19.265954 C 0.129002 10.771015 19.114998 C 0.930405 11.251639 20.315846 S -0.219234 11.851160 21.646332 H -0.533286 9.932377 19.375915 H 1.544552 10.439960 20.723020 H 1.595840 12.073666 20.026522 H 0.735137 12.251503 22.523930 H -0.481183 11.579124 18.686735 H 0.831725 10.429493 18.340616 C 4.023035 15.420899 13.654091 C 4.361019 14.399898 14.739777 S 3.508687 12.776975 14.443149 H 4.541054 16.373684 13.848294 H 5.444603 14.218515 14.778505 H 4.051011 14.757512 15.731295 H 4.330084 15.063513 12.660270 H 2.942215 15.619998 13.621457 C 6.703979 14.930041 19.886970 C 7.267998 13.716321 19.158103 S 6.835971 12.116248 19.998097 H 5.606395 14.885826 19.917430 H 6.882472 13.670467 18.130584 H 8.365897 13.764102 19.103266 H 7.073424 14.977642 20.921764 H 6.995191 15.862390 19.374870	40 Absolute Energy: -3874.241079 Fe 4.157552 9.170956 17.226948 Fe 3.696602 11.567092 16.234848 Fe 5.117496 11.336720 18.524805 S 2.197410 9.780901 16.148840 S 4.222488 9.507814 19.469802 S 5.867291 10.632612 16.460422 S 3.584453 12.936578 18.032540 C 6.183993 6.164027 18.836950 C 6.302294 6.712257 17.417385 S 4.666319 6.967574 16.574137 H 5.607121 6.862139 19.460201 H 6.825143 7.679839 17.426788 H 6.885748 6.025704 16.783959 H 5.675280 5.188392 18.846039 H 7.181085 6.036788 19.293373 C 0.129001 10.771028 19.114979 C 0.954358 11.415550 20.216120 S -0.163395 12.070334 21.553987 H -0.458505 9.918021 19.487425 H 1.639847 10.685972 20.661912 H 1.551143 12.242377 19.811210 H 0.805926 12.570999 22.361595 H -0.559701 11.493190 18.651340 H 0.812209 10.406763 18.329052 C 4.022995 15.420904 13.654046 C 4.508442 14.226825 14.475811 S 3.455377 12.724578 14.205744 H 4.672669 16.298923 13.811411 H 5.546981 13.973471 14.214224 H 4.488846 14.462069 15.549372 H 4.019190 15.188736 12.578236 H 2.997403 15.698667 13.938453 C 6.704012 14.930041 19.887025 C 7.279046 13.713694 19.165537 S 6.779662 12.106806 19.946037 H 5.605436 14.912511 19.853043 H 6.945745 13.691873 18.118962 H 8.379731 13.747903 19.165580 H 7.012882 14.945403 20.943025 H 7.047121 15.866414 19.413997

Table S5 Cartesian coordinates (Å) and total absolute energies (Hartree) of the DFT-optimized models using PW91 functional and BS13 broken-symmetry state.

Oxidized *Pf* Fd D14C [3Fe-4S]$^{1+}$ model $[[Fe_3S_4](CH_3CH_2S)_3(CH_3CH_2SH)]^{2-}$	**Reduced *Pf* Fd D14C [3Fe-4S]^{0} model** $[[Fe_3S_4](CH_3CH_2S)_3(CH_3CH_2SH)]^{3-}$
40 Absolute Energy: -3874.159877 Fe 4.400217 9.281904 16.967370 Fe 3.557816 11.612732 16.140693 Fe 4.985871 11.449915 18.293573 S 2.398253 9.704501 16.140397 S 4.395456 9.551784 19.145964 S 5.787002 10.947429 16.282522 S 3.313308 12.807986 18.045633 C 6.183969 6.163947 18.837083 C 6.577231 6.919305 17.574361 S 5.137342 7.231026 16.451425 H 5.456592 6.747835 19.417888 H 7.023258 7.890909 17.822877 H 7.312599 6.349642 16.986017 H 5.731250 5.191767 18.593729 H 7.065500 5.984262 19.474799 C 0.128990 10.770886 19.115036 C 0.992329 10.921402 20.358975 S -0.052654 11.486011 21.788453 H -0.661202 10.017936 19.254011 H 1.461602 9.968593 20.629390 H 1.781159 11.662303 20.182139 H 0.950660 11.606455 22.694120 H -0.341052 11.725236 18.837089 H 0.768666 10.454800 18.276858 C 4.023024 15.421169 13.653938 C 4.377243 14.210822 14.508658 S 3.157899 12.835866 14.271277 H 4.766352 16.223763 13.789577 H 5.374156 13.826815 14.249907 H 4.389232 14.472969 15.575926 H 3.997001 15.160531 12.585562 H 3.036026 15.820474 13.927118 C 6.704018 14.929999 19.886944 C 7.113305 13.736918 19.024882 S 6.544110 12.112821 19.725267 H 5.609575 14.989913 19.969850 H 6.688902 13.822552 18.015635 H 8.208268 13.684616 18.924147 H 7.116407 14.847052 20.903108 H 7.068515 15.872734 19.446219	40 Absolute Energy: -3874.241290 Fe 4.184847 9.087575 16.987263 Fe 3.650308 11.485492 15.897650 Fe 4.840788 11.298902 18.294117 S 2.355222 9.641913 15.803304 S 4.045348 9.371756 19.299700 S 5.782230 10.677296 16.211911 S 3.276883 12.820577 17.697907 C 6.184058 6.164091 18.836837 C 6.458681 6.770181 17.465465 S 4.928408 6.942775 16.433814 H 5.485346 6.808907 19.388228 H 6.900957 7.769730 17.576727 H 7.169533 6.150901 16.895609 H 5.737371 5.162401 18.745335 H 7.115385 6.076669 19.423855 C 0.128875 10.771084 19.115032 C 0.957818 11.083317 20.350087 S -0.156814 11.649847 21.730787 H -0.599686 9.968185 19.304032 H 1.511744 10.199304 20.684344 H 1.677727 11.880829 20.132514 H 0.812469 11.852632 22.658811 H -0.412054 11.658781 18.756022 H 0.806735 10.443787 18.313856 C 4.023043 15.420764 13.654040 C 4.530348 14.133344 14.294824 S 3.406168 12.701719 13.950529 H 4.719999 16.254290 13.845487 H 5.532839 13.881481 13.918855 H 4.601282 14.242300 15.386343 H 3.918355 15.310620 12.563826 H 3.039523 15.699076 14.058609 C 6.704024 14.930062 19.887091 C 6.930285 13.742653 18.953225 S 6.493616 12.121028 19.745385 H 5.647260 14.984878 20.184849 H 6.317784 13.846612 18.045729 H 7.983955 13.694940 18.638172 H 7.307721 14.835806 20.802277 H 6.973611 15.879915 19.393341

Table S6 Cartesian coordinates (Å) and total absolute energies (Hartree) of the DFT-optimized models using PW91 functional and BS23 broken-symmetry state.

Oxidized *Pf* Fd D14C [3Fe-4S]$^{1+}$ model $[[Fe_3S_4](CH_3CH_2S)_3(CH_3CH_2SH)]^{2-}$	**Reduced *Pf* Fd D14C [3Fe-4S]^{0} model** $[[Fe_3S_4](CH_3CH_2S)_3(CH_3CH_2SH)]^{3-}$
40 Absolute Energy: -3874.159390 Fe 4.404766 9.290284 17.110698 Fe 3.758708 11.717254 16.458522 Fe 5.178110 11.354562 18.524929 S 2.516547 9.910663 16.118947 S 4.285195 9.512021 19.333602 S 5.856383 10.932556 16.367140 S 3.699590 13.004916 18.222535 C 6.183977 6.164070 18.836895 C 6.480111 6.963440 17.572895 S 4.983658 7.192131 16.492362 H 5.445615 6.692330 19.456009 H 6.864436 7.960188 17.830652 H 7.239305 6.461582 16.954483 H 5.785113 5.169028 18.592061 H 7.100717 6.030867 19.435047 C 0.128954 10.771018 19.114948 C 0.824528 11.296038 20.362346 S -0.433884 11.678783 21.675229 H -0.422409 9.841401 19.318346 H 1.524709 10.551399 20.758419 H 1.385422 12.209995 20.134554 H 0.435304 12.100623 22.628228 H -0.572043 11.510596 18.701307 H 0.889422 10.557480 18.347991 C 4.023012 15.420792 13.654154 C 4.247907 14.500260 14.852207 S 3.134928 13.020529 14.785358 H 4.694689 16.292455 13.705691 H 5.284900 14.139101 14.881577 H 4.053426 15.022973 15.798690 H 4.218694 14.896168 12.707837 H 2.987708 15.790644 13.626288 C 6.704057 14.930119 19.887002 C 7.304512 13.740832 19.146474 S 6.804348 12.112876 19.879751 H 5.607080 14.902708 19.826493 H 6.995098 13.741315 18.093157 H 8.404192 13.772127 19.176669 H 6.991122 14.924383 20.948596 H 7.049268 15.878410 19.442326	40 Absolute Energy: -3874.241419 Fe 4.091362 9.118855 17.189488 Fe 3.575420 11.578558 16.227992 Fe 4.793563 11.327353 18.573029 S 2.219493 9.784032 16.138103 S 3.859536 9.466251 19.418807 S 5.713146 10.586156 16.511339 S 3.368167 13.085775 18.005075 C 6.183988 6.164018 18.837014 C 6.236129 6.654876 17.393731 S 4.565423 6.926777 16.632219 H 5.685404 6.907592 19.473932 H 6.786696 7.603504 17.333944 H 6.756170 5.924759 16.753873 H 5.629842 5.216636 18.916253 H 7.202561 6.001528 19.229604 C 0.129017 10.770990 19.114991 C 0.799589 11.391007 20.328718 S -0.482696 11.937471 21.564756 H -0.449940 9.872723 19.379050 H 1.467285 10.669142 20.812457 H 1.392389 12.262255 20.025463 H 0.369338 12.496242 22.461263 H -0.539704 11.486487 18.614154 H 0.910330 10.479637 18.394919 C 4.022993 15.421011 13.654006 C 4.506190 14.222283 14.467407 S 3.437645 12.735122 14.205119 H 4.684236 16.292309 13.801153 H 5.539478 13.960325 14.193143 H 4.495282 14.442525 15.544255 H 4.000698 15.189123 12.578228 H 3.005108 15.710287 13.953655 C 6.704001 14.929981 19.886991 C 7.119026 13.654016 19.157761 S 6.492260 12.117481 19.982365 H 5.608750 15.016137 19.897422 H 6.729266 13.659296 18.131310 H 8.216344 13.580709 19.099689 H 7.057497 14.921058 20.929031 H 7.117917 15.824319 19.389001

Table S7 Cartesian coordinates (Å) and total absolute energies (Hartree) of the DFT-optimized models using B(5HF)B86 functional and BS12 broken-symmetry state.

Oxidized *Pf* Fd D14C [3Fe-4S]$^{1+}$ model $[[Fe_3S_4](CH_3CH_2S)_3(CH_3CH_2SH)]^{2-}$	**Reduced *Pf* Fd D14C [3Fe-4S]^{0} model** $[[Fe_3S_4](CH_3CH_2S)_3(CH_3CH_2SH)]^{3-}$
40 Absolute Energy: -3874.692326 Fe 4.435423 9.256407 17.253565 Fe 3.968600 11.666010 16.331863 Fe 5.221537 11.348179 18.649326 S 2.752460 9.823525 16.026482 S 4.262356 9.460068 19.429236 S 6.026320 10.672396 16.560073 S 3.655003 12.907543 18.145794 C 6.183984 6.164044 18.836942 C 6.341252 6.706885 17.417887 S 4.738308 7.165090 16.599896 H 5.725420 6.925905 19.484646 H 6.983743 7.598967 17.411056 H 6.807714 5.955923 16.759327 H 5.543618 5.268845 18.851089 H 7.166162 5.893514 19.261212 C 0.129002 10.771015 19.114998 C 0.904121 11.265408 20.330032 S -0.277286 11.845168 21.642561 H -0.520393 9.917949 19.365210 H 1.525342 10.463502 20.747839 H 1.561209 12.098392 20.050720 H 0.654084 12.248940 22.542655 H -0.492453 11.568252 18.679994 H 0.847999 10.444431 18.347602 C 4.023035 15.420899 13.654091 C 4.325723 14.405820 14.757653 S 3.453356 12.793407 14.454329 H 4.549183 16.370080 13.850297 H 5.406318 14.210131 14.817692 H 4.003047 14.780432 15.739227 H 4.346649 15.050280 12.669293 H 2.944704 15.633507 13.597260 C 6.703979 14.930041 19.886970 C 7.310327 13.711244 19.198005 S 6.862642 12.114638 20.038863 H 5.605863 14.879535 19.865758 H 6.973292 13.652656 18.153686 H 8.409893 13.768761 19.191908 H 7.024344 14.991810 20.938294 H 7.014260 15.859242 19.378057	40 Absolute Energy: -3874.787770 Fe 4.155483 9.139226 17.208109 Fe 3.689263 11.549845 16.212416 Fe 5.132520 11.329624 18.538052 S 2.198224 9.760154 16.129697 S 4.224120 9.493042 19.465180 S 5.869861 10.616150 16.456876 S 3.591709 12.923409 18.028607 C 6.183993 6.164027 18.836950 C 6.305775 6.667611 17.398911 S 4.669845 6.923633 16.553082 H 5.626787 6.893476 19.443246 H 6.845001 7.626823 17.378324 H 6.876534 5.952471 16.784300 H 5.653375 5.199734 18.878278 H 7.182023 6.027574 19.291427 C 0.129001 10.771028 19.114979 C 0.940753 11.416860 20.228390 S -0.196130 12.073826 21.550540 H -0.464086 9.917867 19.481138 H 1.620083 10.687572 20.686055 H 1.543088 12.244006 19.830875 H 0.760229 12.584506 22.366877 H -0.554939 11.493960 18.643380 H 0.819858 10.405533 18.335962 C 4.022995 15.420904 13.654046 C 4.513002 14.215763 14.459708 S 3.454291 12.718151 14.178516 H 4.674903 16.297482 13.817926 H 5.549993 13.965089 14.186880 H 4.501170 14.440153 15.536353 H 4.013285 15.201038 12.574596 H 2.998520 15.696867 13.947457 C 6.704012 14.930041 19.887025 C 7.288777 13.714649 19.168149 S 6.803515 12.105439 19.955586 H 5.604774 14.904152 19.856094 H 6.955697 13.687651 18.121015 H 8.389904 13.757673 19.167262 H 7.016000 14.952514 20.943089 H 7.038666 15.868162 19.409048

Table S8 Cartesian coordinates (Å) and total absolute energies (Hartree) of the DFT-optimized models using B(5HF)B86 functional and BS13 broken-symmetry state.

Oxidized *Pf* Fd D14C [3Fe-4S]$^{1+}$ model $[[Fe_3S_4](CH_3CH_2S)_3(CH_3CH_2SH)]^{2-}$	**Reduced *Pf* Fd D14C [3Fe-4S]^{0} model** $[[Fe_3S_4](CH_3CH_2S)_3(CH_3CH_2SH)]^{3-}$
40 Absolute Energy: -3874.691582 Fe 4.231580 9.165947 16.891679 Fe 3.473468 11.512716 15.888978 Fe 4.732790 11.363807 18.190505 S 2.295143 9.605661 15.879208 S 4.237996 9.472770 19.114899 S 5.683753 10.830629 16.262722 S 3.102770 12.749801 17.762765 C 6.183959 6.163954 18.837070 C 6.510280 6.903303 17.544314 S 5.032081 7.104931 16.445918 H 5.443282 6.727677 19.421982 H 6.909971 7.903402 17.758374 H 7.264087 6.356509 16.956074 H 5.773621 5.164311 18.629144 H 7.089306 6.043117 19.457212 C 0.129016 10.770900 19.115029 C 0.869656 10.815661 20.445380 S -0.324279 11.207017 21.816670 H -0.646718 9.989701 19.107039 H 1.342870 9.850899 20.663805 H 1.646871 11.588931 20.424761 H 0.574153 11.212716 22.833415 H -0.343980 11.738373 18.887678 H 0.847505 10.554907 18.309941 C 4.023018 15.421142 13.653947 C 4.436880 14.138490 14.367667 S 3.295284 12.730912 13.968486 H 4.727225 16.238321 13.886021 H 5.454715 13.840922 14.076129 H 4.430394 14.276671 15.458480 H 4.011168 15.284534 12.561479 H 3.016840 15.739586 13.964863 C 6.704007 14.930004 19.886954 C 6.728548 13.772909 18.886669 S 6.173078 12.175784 19.654469 H 5.682938 15.104611 20.256882 H 6.060712 13.976936 18.038772 H 7.743203 13.620428 18.487416 H 7.347908 14.722038 20.755435 H 7.062858 15.859423 19.412999	40 Absolute Energy: -3874.787662 Fe 4.180530 9.073751 16.948592 Fe 3.572684 11.485139 15.825285 Fe 4.817133 11.303666 18.249535 S 2.308495 9.608381 15.789057 S 4.047711 9.373535 19.262981 S 5.727086 10.704739 16.128966 S 3.236672 12.822655 17.643623 C 6.184058 6.164091 18.836837 C 6.491812 6.774974 17.472747 S 4.989038 6.937760 16.399835 H 5.481096 6.811154 19.381707 H 6.929112 7.775543 17.598542 H 7.221469 6.158937 16.921785 H 5.730994 5.165754 18.730005 H 7.104247 6.064186 19.441484 C 0.128875 10.771084 19.115032 C 0.969618 11.097276 20.340623 S -0.135287 11.666413 21.729396 H -0.592147 9.963176 19.317008 H 1.532126 10.217818 20.674873 H 1.682994 11.897956 20.109176 H 0.840466 11.887465 22.645938 H -0.423927 11.653391 18.757598 H 0.798959 10.444091 18.305494 C 4.023043 15.420764 13.654040 C 4.525295 14.092777 14.216331 S 3.341784 12.708538 13.869941 H 4.751757 16.228452 13.844199 H 5.499252 13.828068 13.777933 H 4.654318 14.154023 15.307208 H 3.861787 15.358794 12.565876 H 3.067572 15.704704 14.120638 C 6.704024 14.930062 19.887091 C 6.906778 13.758523 18.924662 S 6.482181 12.126051 19.701334 H 5.655374 14.980835 20.214902 H 6.276552 13.882578 18.031623 H 7.954358 13.715334 18.586573 H 7.332779 14.819126 20.784660 H 6.961879 15.889894 19.403990

Table S9 Cartesian coordinates (Å) and total absolute energies (Hartree) of the DFT-optimized models using B(5HF)B86 functional and BS23 broken-symmetry state.

Oxidized *Pf* Fd D14C [3Fe-4S]$^{1+}$ model $[[Fe_3S_4](CH_3CH_2S)_3(CH_3CH_2SH)]^{2-}$	**Reduced *Pf* Fd D14C [3Fe-4S]^{0} model** $[[Fe_3S_4](CH_3CH_2S)_3(CH_3CH_2SH)]^{3-}$
40 Absolute Energy: -3874.692308 Fe 4.374489 9.249848 17.094312 Fe 3.719352 11.713823 16.469746 Fe 5.164126 11.359056 18.523795 S 2.485606 9.900417 16.093402 S 4.287395 9.493936 19.329593 S 5.815941 10.923972 16.343526 S 3.678847 13.020545 18.217138 C 6.183977 6.164070 18.836895 C 6.493268 6.956614 17.570029 S 5.013309 7.158978 16.460349 H 5.426393 6.687002 19.438214 H 6.864635 7.959087 17.826605 H 7.268699 6.457344 16.968522 H 5.804149 5.160030 18.593719 H 7.092146 6.049510 19.453729 C 0.128954 10.771018 19.114948 C 0.819362 11.292861 20.369092 S -0.446376 11.679904 21.675005 H -0.431745 9.845180 19.315572 H 1.514558 10.544322 20.768872 H 1.385434 12.205382 20.144614 H 0.417290 12.094709 22.635729 H -0.563658 11.515964 18.694496 H 0.893865 10.549873 18.353585 C 4.023012 15.420792 13.654154 C 4.229408 14.515961 14.869399 S 3.103899 13.046087 14.804512 H 4.700500 16.289690 13.700295 H 5.264450 14.148964 14.913380 H 4.028894 15.055978 15.805439 H 4.225505 14.880967 12.716782 H 2.989694 15.797892 13.609936 C 6.704057 14.930119 19.887002 C 7.303581 13.745371 19.135326 S 6.816455 12.112142 19.867584 H 5.605806 14.897750 19.837563 H 6.985733 13.749679 18.083931 H 8.404185 13.781516 19.155623 H 7.001971 14.921673 20.946667 H 7.040426 15.883031 19.442664	40 Absolute Energy: -3874.787481 Fe 4.089323 9.066785 17.218979 Fe 3.614501 11.572076 16.247546 Fe 4.810317 11.312498 18.625777 S 2.239897 9.776257 16.140224 S 3.852530 9.437573 19.453432 S 5.738431 10.534807 16.569417 S 3.396566 13.067792 18.026116 C 6.183988 6.164018 18.837014 C 6.191433 6.516259 17.350313 S 4.507478 6.854340 16.647051 H 5.789137 7.005368 19.424511 H 6.816751 7.402237 17.168509 H 6.611138 5.686586 16.758446 H 5.553721 5.282160 19.032810 H 7.207388 5.944016 19.190356 C 0.129017 10.770990 19.114991 C 0.788090 11.384127 20.341473 S -0.510239 11.934090 21.560433 H -0.458019 9.874182 19.369933 H 1.444415 10.655768 20.832690 H 1.391629 12.252785 20.049215 H 0.328174 12.488701 22.471797 H -0.531626 11.492141 18.609527 H 0.916547 10.477669 18.401803 C 4.022993 15.421011 13.654006 C 4.543630 14.227608 14.456041 S 3.500177 12.719570 14.200287 H 4.663114 16.309231 13.801685 H 5.578644 13.989606 14.163809 H 4.545129 14.446660 15.533422 H 3.998994 15.194479 12.576067 H 2.999309 15.681763 13.962554 C 6.704001 14.929981 19.886991 C 7.151365 13.642246 19.193897 S 6.529823 12.109384 20.033029 H 5.606724 15.000663 19.881165 H 6.788682 13.622089 18.156974 H 8.251517 13.583901 19.163304 H 7.042379 14.952321 20.934928 H 7.112228 15.819087 19.372961

References

1 D. Mitra, V. Pelmenschikov, Y. Guo, D. A. Case, H. Wang, W. Dong, M. L. Tan, T. Ichiye, F. E. Jenney, M. W. Adams, Y. Yoda, J. Zhao and S. P. Cramer, *Biochemistry*, 2011, **50**, 5220-5235.

2 K. Lagarec and D. C. Rancourt, *Recoil, Mössbauer Spectral Analysis Software for Windows, 1.0. Department of Physics, University of Ottawa, Canada*, 1998.

3 L. Lauterbach, H. Wang, M. Horch, L. B. Gee, Y. Yoda, Y. Tanaka, I. Zebger, O. Lenz and S. P. Cramer, *Chem. Sci.*, 2015, **6**, 1055-1060.

4 W. Sturhahn, *J. Phys. Condens. Mat.*, 2004, **16**, S497-S530.

5 M. N. Løvgreen, M. Martic, M. S. Windahl, H. E. Christensen and P. Harris, *J. Biol. Inorg. Chem.*, 2011, **16**, 763-775.

6 P. J. Stephens, G. M. Jensen, F. J. Devlin, T. V. Morgan, C. D. Stout, A. E. Martin and B. K. Burgess, *Biochemistry*, 1991, **30**, 3200-3209.

7 L. Noodleman and D. A. Case, *Adv. Inorg. Chem.*, 1992, **38**, 423-470.

8 B. Friedrich, J. Fritsch and O. Lenz, *Curr. Opin. Biotech.*, 2011, **22**, 358-364.

9 M. J. Frisch, G. W. Trucks, H. B. Schlegel, G. E. Scuseria, M. A. Robb, J. R. Cheeseman, G. Scalmani, V. Barone, B. Mennucci, G. A. Petersson, H. Nakatsuji, M. Caricato, X. Li, H. P. Hratchian, A. F. Izmaylov, J. Bloino, G. Zheng, J. L. Sonnenberg, M. Hada, M. Ehara, K. Toyota, R. Fukuda, J. Hasegawa, M. Ishida, T. Nakajima, Y. Honda, O. Kitao, H. Nakai, T. Vreven, J. A. Montgomery, Jr., J. E. Peralta, F. Ogliaro, M. Bearpark, J. J. Heyd, E. Brothers, K. N. Kudin, V. N. Staroverov, R. Kobayashi, J. Normand, K. Raghavachari, A. Rendell, J. C. Burant, S. S. Iyengar, J. Tomasi, M. Cossi, N. Rega, J. M. Millam, M. Klene, J. E. Knox, J. B. Cross, V. Bakken, C. Adamo, J. Jaramillo, R. Gomperts, R. E. Stratmann, O. Yazyev, A. J. Austin, R. Cammi, C. Pomelli, J. W. Ochterski, R. L. Martin, K. Morokuma, V. G. Zakrzewski, G. A. Voth, P. Salvador, J. J. Dannenberg, S. Dapprich, A. D. Daniels, Ö. Farkas, J. B. Foresman, J. V. Ortiz, J. Cioslowski and D. J. Fox, *Gaussian 09, Revision D.01, Gaussian Inc., Wallingford CT, 2009*.

10 D. Mitra, S. J. George, Y. Guo, S. Kamali, S. Keable, J. W. Peters, V. Pelmenschikov, D. A. Case and S. P. Cramer, *J. Am. Chem. Soc.*, 2013, **135**, 2530-2543.

11 J. Tomasi, B. Mennucci and R. Cammi, *Chem. Rev.*, 2005, **105**, 2999-3093.

12 K. P. Jensen, *J. Inorg. Biochem.*, 2008, **102**, 87-100.

13 K. P. Jensen, B. L. Ooi and H. E. M. Christensen, *Inorg. Chem.*, 2007, **46**, 8710-8716.

14 J. P. Perdew, J. A. Chevary, S. H. Vosko, K. A. Jackson, M. R. Pederson, D. J. Singh and C. Fiolhais, *Phys. Rev. B*, 1992, **46**, 6671-6687.

15 T. V. Harris and R. K. Szilagyi, *J. Comput. Chem.*, 2014, **35**, 540-552.

16 R. K. Szilagyi and M. A. Winslow, *J. Comput. Chem.*, 2006, **27**, 1385-1397.

17 A. D. Becke, *Phys. Rev. A*, 1988, **38**, 3098-3100.

18 J. P. Perdew, *Phys. Rev. B*, 1986, **33**, 8822-8824.

19 V. Pelmenschikov and M. Kaupp, *J. Am. Chem. Soc.*, 2013, **135**, 11809-11823.

20 F. Neese, *Coord. Chem. Rev.*, 2009, **253**, 526-563.

21 K. P. Jensen, B. L. Ooi and H. E. M. Christensen, *J. Phys. Chem. A*, 2008, **112**, 12829-12841.

22 A. D. Scott, V. Pelmenschikov, Y. S. Guo, L. F. Yan, H. X. Wang, S. J. George, C. H. Dapper, W. E. Newton, Y. Yoda, Y. Tanaka and S. P. Cramer, *J. Am. Chem. Soc.*, 2014, **136**, 15942-15954.

23 D. Schilter, V. Pelmenschikov, H. X. Wang, F. Meier, L. B. Gee, Y. Yoda, M. Kaupp, T. B. Rauchfuss and S. P. Cramer, *Chem. Commun.*, 2014, **50**, 13469-13472.

24 L. F. Yan, V. Pelmenschikov, C. H. Dapper, A. D. Scott, W. E. Newton and S. P. Cramer, *Chem. Eur. J.*, 2012, **18**, 16349-16357.

25 V. Pelmenschikov, Y. S. Guo, H. X. Wang, S. P. Cramer and D. A. Case, *Farad. Discuss.*, 2011, **148**, 409-420.

26 T. A. Kent, B. H. Huynh and E. Münck, *Proc. Natl. Acad. Sci. U. S. A.*, 1980, **77**, 6574-6576.

27 V. Papaefthymiou, J. J. Girerd, I. Moura, J. J. G. Moura and E. Munck, *J. Am. Chem. Soc.*, 1987, **109**, 4703-4710.

28 M. E. Pandelia, N. D. Lanz, S. J. Booker and C. Krebs, *Biochim. Biophys. Acta*, 2015, **1853**, 1395-1405.

29 A. Dey, T. Glaser, J. J. G. Moura, R. H. Holm, B. Hedman, K. O. Hodgson and E. I. Solomon, *J. Am. Chem. Soc.*, 2004, **126**, 16868-16878.

30 R. E. Duderstadt, C. R. Staples, P. S. Brereton, M. W. W. Adams and M. K. Johnson, *Biochemistry*, 1999, **38**, 10585-10593.

31 A. Donaire, C. M. Gorst, Z. H. Zhou, M. W. W. Adams and G. N. Lamar, *J. Am. Chem. Soc.*, 1994, **116**, 6841-6849.

32 M. S. Nielsen, P. Harris, B. L. Ooi and H. E. Christensen, *Biochemistry*, 2004, **43**, 5188-5194.

33 C. G. Schipke, D. B. Goodin, D. E. McRee and C. D. Stout, *Biochemistry*, 1999, **38**, 8228-8239.

34 C. D. Stout, E. A. Stura and D. E. McRee, *J. Mol. Biol.*, 1998, **278**, 629-639.

35 J. Zhou, Z. G. Hu, E. Munck and R. H. Holm, *J. Am. Chem. Soc.*, 1996, **118**, 1966-1980.

36 M. H. M. Olsson, U. Ryde and B. O. Roos, *Protein Sci.*, 1998, **7**, 2659-2668.

37 E. Sigfridsson, M. H. M. Olsson and U. Ryde, *Inorg. Chem.*, 2001, **40**, 2509-2519.

38 J. G. Reynolds, C. L. Coyle and R. H. Holm, *J. Am. Chem. Soc.*, 1980, **102**, 4350-4355.